

Fuel Performance Modeling Results for Representative FCRD Irradiation Experiments: Projected Deformation in the Annular AFC-3A U-10Zr Fuel Pins and Comparison to Alternative Designs

Pavel Medvedev

September 2012

The INL is a U.S. Department of Energy National Laboratory
operated by Battelle Energy Alliance



DISCLAIMER

This information was prepared as an account of work sponsored by an agency of the U.S. Government. Neither the U.S. Government nor any agency thereof, nor any of their employees, makes any warranty, expressed or implied, or assumes any legal liability or responsibility for the accuracy, completeness, or usefulness, of any information, apparatus, product, or process disclosed, or represents that its use would not infringe privately owned rights. References herein to any specific commercial product, process, or service by trade name, trade mark, manufacturer, or otherwise, does not necessarily constitute or imply its endorsement, recommendation, or favoring by the U.S. Government or any agency thereof. The views and opinions of authors expressed herein do not necessarily state or reflect those of the U.S. Government or any agency thereof.

**Fuel Performance Modeling Results for
Representative FCRD Irradiation Experiments:
Projected Deformation in the Annular AFC-3A U-10Zr
Fuel Pins and Comparison to Alternative Designs**

Pavel Medvedev

September 2012

**Idaho National Laboratory
Idaho Falls, Idaho 83415**

<http://www.inl.gov>

**Prepared for the
U.S. Department of Energy
Office of Nuclear Energy
Under DOE Idaho Operations Office
Contract DE-AC07-05ID14517**

INTENTIONALLY BLANK

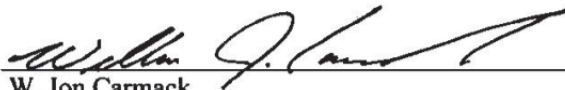
Fuel Cycle Research and Development Advanced Fuels Campaign

**Fuel Performance Modeling Results for
Representative FCRD Irradiation Experiments:
Projected Deformation in the Annular AFC-3A U-10Zr
Fuel Pins and Comparison to Alternative Designs**

INL/EXT-12-27183
Revision 1

September 2012

Approved by:



W. Jon Carmack
Deputy National Technical Director
Advanced Fuels Campaign

Sept 17, 2012

Date

INTENTIONALLY BLANK

SUMMARY

The objective of the present study was to predict the outcome of the AFC-3A annular U-10Zr fuel irradiation experiment. Specifically, the study attempted to predict whether the annular fuel will swell inward and fill the annulus, or swell outward resulting in an undesirable cladding deformation.

It was predicted that both 55% and 75% annular fuels operating at 350 W/cm for 201 days will swell inward and partially fill the annulus which signifies a positive outcome of the experiment. The driving mechanism for such behavior is the fuel creep under the compressive stress exerted on the fuel by the cladding as a result of the fuel cladding mechanical interaction.

Comparison with the solid fuel revealed that the annular fuel is expected to swell less early in life due to the mechanical constraint provided by the cladding. Furthermore, mechanical constraint is expected to yield a marked reduction of the axial elongation of the annular fuel as compared to the solid fuel. The prediction is based on the assumption that the annular fuel is not capable of moving axially relative to the cladding after the two come in contact. Post irradiation examination results would be very useful to assess the validity of this assumption. Specifically, underprediction of the axial growth would point to the fact that some slippage of the fuel relative to the cladding occurs after the onset of the FCMI.

As fuel creep plays the major role in the deformation of the annular fuel, the contributions from the thermal and irradiation induced creep to the total creep rate of fuel were examined to provide guidance for possible creep testing experiments of the fuel (separate effect tests). It was found that irradiation induced creep dominates deformation of the fresh fuel at low temperatures. At high temperatures, and in the case of porous fuel, the thermal creep of the fuel becomes dominant and irradiation induced creep can be neglected. Fission gas induced porosity seems to accelerate fuel creep drastically. Recognizing the sensitivity of the fuel creep to the porosity, additional studies exploring this phenomenon and verifying published equations either experimentally or through computation may benefit the understanding of the annular fuel behavior.

INTENTIONALLY BLANK

CONTENTS

SUMMARY	vii
1. OBJECTIVE.....	1
2. BACKGROUND.....	1
2.1 Description of the BISON Fuel Performance Code.....	1
2.2 AFC-3A Annular U-10Zr Fuel Irradiation Experiment Design and Operating Conditions	1
3. PROBLEM STATEMENT	2
4. MODELS DEVELOPED AND IMPLEMENTED IN BISON BY THE PRESENT STUDY.....	3
4.1 Mechanistic Fuel Swelling Model	3
4.1.1 Fuel Swelling Due to Fission Gas and Fission Gas Release.....	3
4.1.2 Fuel swelling due to solid fission products	4
4.2 Degradation of the Fuel Thermal Conductivity	4
4.3 Fuel Creep.....	4
4.4 Cladding Creep	4
4.5 Coupling Between the Models to Capture the Multiphysics Phenomena.....	5
5. CALCULATION PROCEDURE.....	5
5.1 Mesh Files.....	5
5.2 Input Files	6
5.3 Assumptions and Limitations.....	7
5.4 Computer Platforms and Software Version	7
5.5 Code Verification.....	7
6. RESULTS.....	8
6.1 Fuel Swelling and Fission Gas Release	8
6.2 Fuel and Cladding Temperature.....	11
6.3 Cladding Stress	12
6.4 Plenum Pressure.....	12
6.5 Dominant Fuel Creep Mechanism	13
6.5.1 Beginning of Life, Non-porous Fuel.....	13
6.5.2 Effect of Fuel Porosity	14
6.6 Fuel Creep Strain	15
6.7 Comparison with the Annular 75% SD U-10Zr Fuel.....	16
6.8 Comparison with the Solid 55% SD U-10Zr Fuel	18
7. CONCLUSIONS	22
8. REFERENCES	23

FIGURES

Figure 1. A schematic of the AFC-3A annular rodlet assembly	2
Figure 2. A schematic of the AFC-3 annular fuel slug.	2
Figure 3. Coupling between the models to capture the multiphysics phenomena	5
Figure 4. A diagram of the QUAD8 element used in the rodlet assembly mesh.	6
Figure 5. Results for the simulation of the AFC-3A annular U-10Zr fuel irradiation where (a) shows fuel and cladding geometry before the irradiation, (b) shows fuel and cladding geometry after irradiation.	8
Figure 6. Evolution of the fuel annulus, fuel outer diameter, and cladding outer diameter at the fuel mid-plane as a function of burnup.....	9
Figure 7. Fuel axial elongation as a function of burnup.	9
Figure 8. Evolution of the hydrostatic stress with the fuel with burnup. The data is for an element located at the midplane on the exterior surface of the fuel slug.	10
Figure 9. Fuel swelling as a function of burnup.	10
Figure 10. Fission gas release as a function of burnup.	11
Figure 11. History of the peak fuel and peak cladding temperatures.....	11
Figure 12. Evolution of the cladding mid-wall hoop stress at the fuel mid-plane.	12
Figure 13. Plenum pressure history.....	13
Figure 14. Contributions from thermal and irradiation induced creep to the total creep rate of the fuel at 600C, non-porous fuel.	13
Figure 15. Contributions from thermal and irradiation induced creep to the total creep rate of the fuel at 726C, non-porous fuel.	14
Figure 16. Contributions from thermal and irradiation induced creep to the total creep rate of the fuel at 600C, fuel porosity 26%.....	14
Figure 17. Contributions from thermal and irradiation induced creep to the total creep rate of the fuel at 726C, fuel porosity 26%.....	15
Figure 18. Fuel creep strain at the end of irradiation.	15
Figure 19. Results for the simulation of the annular 75% U-10Zr fuel irradiation where (a) shows fuel and cladding geometry before the irradiation, (b) shows fuel and cladding geometry after irradiation.	16
Figure 20. Comparison of the swelling of the annular 55% and 75% SD fuel.	17
Figure 21. Comparison of the hydrostatic stress in the annular 55% and 75% SD fuel.	17
Figure 22. Comparison of the fission gas release in the annular 55% and 75% SD fuel.	18
Figure 23. Comparison of the peak fuel temperature in the annular 55% and 75% SD fuel.	18
Figure 24. Fuel and cladding geometry before and after irradiation for the solid 55% U-10Zr fuel.....	19
Figure 25. Swelling comparison of the solid and annular fuels, both fuels 55 %SD.....	19
Figure 26. Peak fuel temperature comparison of the solid and annular fuels, both fuels 55% SD.....	20

Figure 27. Hydrostatic stress comparison in the solid and annular fuels, both fuels 55% SD..... 20

Figure 28. Comparison of the axial fuel elongation of the solid and annular fuels, both fuels 55
%SD..... 21

Figure 29. Fission gas release comparison in the solid and annular fuels, both fuels 55% SD. 21

TABLES

Table 1. Design and operating conditions of the AFC-3A annular U-10Zr irradiation experiment 2

Table 2. Key parameters of the mesh used for the rodlet assembly model..... 6

Table 3. Rodlet assembly dimensions used to generate metal rodlet mesh files. 6

Table 4. Material properties used in the present study..... 7

INTENTIONALLY BLANK

Projected Deformation in the Annular AFC-3A U-10Zr Fuel Pins

1. OBJECTIVE

The primary objective of this work at the Idaho National Laboratory (INL) is to determine the mode of deformation of the annular U-10Zr metallic alloy fuel pin being irradiated in the AFC-3A experiment. Specifically, the study attempts to determine whether the annular fuel slug irradiated in the AFC-3A experiment will swell inward and fill the annulus, or swell outward resulting in an undesirable cladding deformation. The secondary objective is to identify material properties, fuel behavior phenomena, and fuel design parameters that govern the deformation mode of the fuel in the annular configuration. In order to accomplish the secondary objective, the effect of smeared density (SD) on the deformation of the annular fuel is explored, and a comparison to the deformation of the fuel featuring a solid slug design is performed.

This work constitutes a research and development activity that is exploratory, preliminary, or investigative in nature.

2. BACKGROUND

2.1 Description of the BISON Fuel Performance Code

The fuel performance modeling effort described in the present report was executed using the BISON fuel performance code. BISON¹ is a finite element-based engineering scale fuel performance code based on the Multiphysics Object-Oriented Simulation Environment (MOOSE) framework.² BISON solves the fully-coupled thermomechanics and species diffusion equations in two or three dimensional space. The code is currently under development and is being actively advanced by including multiphysics constitutive behavior models, and coupling to lower-length scale material models. Applicable to both steady and transient operation, BISON is designed for efficient use on parallel computers. Current applications include oxide, metal, and tristructural-isotropic (TRISO) nuclear fuels.

BISON employs an object-oriented architecture which minimizes the programming required to add new material and behavior models. This feature was utilized extensively by the present study to develop capabilities to predict swelling, fission gas release, creep, and thermal conductivity degradation in metallic fuel. Detailed description of these capabilities is given in Section 4.

2.2 AFC-3A Annular U-10Zr Fuel Irradiation Experiment Design and Operating Conditions

The motivation for the AFC-3 series experiments is the development of the advanced ultra-high burnup SFR metallic fuel concepts.³ The irradiation experiment seeks to investigate advanced fuel designs with the following features: decreased fuel smeared density (SD), venting of the fission gas to the sodium coolant, a uranium-molybdenum (UMo) based alloy fuel system, coating or liner on the cladding inner surface, and/or targeted fuel alloy additions to reduce fuel-cladding chemical interaction, and an advanced fabrication method that includes consideration of annular fuel and co-extruded fuel and cladding. The AFC-3A annular U-10Zr rodlet addresses the latter concept of the annular fuel coextruded with the cladding. Extrusion of metallic fuel alloy within cladding during fabrication could dramatically reduce process waste, eliminate volatile constituent losses during fabrication, and eliminate need for sodium bond. The behavior of the low SD annular fuel early in life as initial fuel swelling occurs is identified as a principal area of uncertainty in the overview of the project.³

AFC-3A experiment design and operating conditions are described in detail in the experiment thermal evaluation,⁴ and the as-run and projected physics evaluations.⁵ Design and operating conditions information critical for the execution of the present study are summarized in Table 1. Detailed dimensions of the AFC-3 annular fuel rodlet assembly are given in the corresponding engineering drawings.^{6,7} A schematic of the AFC-3A annular rodlet assembly is given in Figure 1. A schematic of the AFC-3 annular fuel slug is given in Figure 2.

Table 1. Design and operating conditions of the AFC-3A annular U-10Zr irradiation experiment.

Rodlet	Composition	Density (g/cm ³)	Irradiation time (days)	LHGR (W/cm)	Fuel outer diameter (cm)	Fuel inner diameter (cm)	Fuel-cladding He gap (microns)	Smeared density
3A-R4	U-10Zr	15.73	201	350	0.493	0.330	34	55%

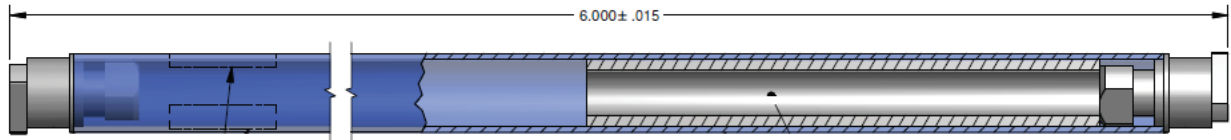


Figure 1. A schematic of the AFC-3A annular rodlet assembly

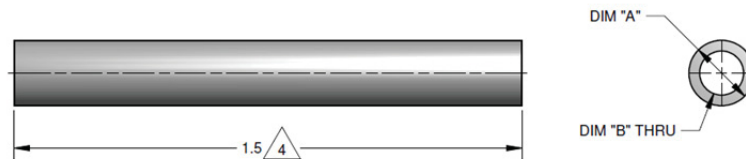


Figure 2. A schematic of the AFC-3 annular fuel slug.

3. PROBLEM STATEMENT

Given the power history, material properties, and rodlet assembly design determine whether the annular U-10Zr fuel slug irradiated in the AFC-3A experiment will swell inward and fill the annulus, or swell outward resulting in an undesirable cladding deformation, identify material properties, fuel behavior phenomena, and fuel design parameters that govern the deformation mode of the fuel in the annular configuration. Compare initial swelling behavior of the annular 55% SD fuel (base design) with that of the 55% solid fuel and 75% solid and annular fuels of the same composition and operating at the same linear power.

4. MODELS DEVELOPED AND IMPLEMENTED IN BISON BY THE PRESENT STUDY

4.1 Mechanistic Fuel Swelling Model

4.1.1 Fuel Swelling Due to Fission Gas and Fission Gas Release

To assess the swelling of the annular fuel early in life, a mechanistic fuel swelling model was developed and implemented in the BISON code. The derivation of the swelling model is presented herein.

Assume that the fission gas generated in the fuel instantly forms fission gas bubbles having diameter of 5 μm . Mechanical force balance on an equilibrium bubble can be expressed as follows.⁸

$$p = \frac{2\gamma}{r_b} - \sigma_h + \sigma_{cr}, \quad (1)$$

where p is the pressure of the fission gas in a bubble, γ surface tension of the fuel, r_b is the fission gas bubble size, σ_h is the hydrostatic stress in the fuel, and σ_{cr} is the creep strength stress of the fuel. The gas pressure in the bubble is governed by the ideal gas law:

$$pV = \nu RT, \quad (2)$$

where p , V , ν , R , T , are pressure, volume, amount, universal gas constant, and temperature of the fission gas, respectively.

Rearranging Equation (2) to calculate volume of the fission gas and substituting Equation (1), obtain the following expression for the volume of the fission gas:

$$V = \frac{\nu RT}{\frac{2\gamma}{r_b} - \sigma_h + \sigma_{cr}}. \quad (3)$$

Amount of the of fission gas generated per unit volume of fuel:

$$\nu = \frac{0.26F}{N_A}, \quad (4)$$

where F is fission density, 0.26 is fission yield of gas atoms, N_A is the Avogadro number. Substituting

$$r_b = 0.5 \mu\text{m},$$

$$\gamma = 0.8 \text{ N/m}, \text{ according to Karahan,}^9$$

$$\sigma_{cr} = 6.9 \times 10^6 \text{ Pa}, \text{ from Churchman}^{10} \text{ for pure U},$$

obtain fuel swelling due to fission gas:

$$\left(\frac{\Delta V}{V_0}\right)_g = \frac{3.59 \times 10^{-24} FT}{1.01 \times 10^7 - \sigma_h}, \quad (5)$$

where T is in degrees Kelvin, F is in fissions/ m^3 , σ_h is in Pa.

According to Barnes,⁸ when swelling due to fission gas bubbles reaches 33%, the fission gas bubbles interconnect, and the fission gas is released. Interconnection of the fission gas bubbles transforms closed porosity into the open porosity that facilitates instant release of any consequently generated fission gas. Thus, the fission gas induced swelling is terminated, once the interconnection threshold is reached. These phenomena were implemented in the code by limiting maximum attainable fission gas induced swelling to 33%, and setting fission gas release value to 80%, once the interconnection threshold is reached. The

latter value is based on the assumption that 20% of the fission gas is retained in isolated bubbles once the rest of the bubbles interconnect. This methodology is expressed as follows:

$$if \left(\frac{\Delta V}{V_0} \right)_g > 0.33, FGR = 80\% \quad (6)$$

4.1.2 Fuel swelling due to solid fission products

Swelling due to solid fission products is assumed to be 1.5% per 1% burnup.¹¹ Noting that

$$Bu(\%) = \frac{F}{N_{hm0}} 100, \quad (7)$$

where N_{hm0} is initial number of heavy metal atoms in the fuel and F is fission density, the swelling due to solid fission products expressed in terms of the fission density is

$$\left(\frac{\Delta V}{V_0} \right)_s = 0.015 Bu(\%) = 0.015 \frac{F}{N_{hm0}} 100 = 0.015 \frac{F}{3.6 \times 10^{28}} 100 = 4.16 \times 10^{-29} F. \quad (8)$$

4.2 Degradation of the Fuel Thermal Conductivity

To account for degradation of thermal conductivity due to the fission gas induced porosity, a methodology developed by Billone¹² was adopted.

$$k = (9.38 \times 10^{-6} T^2 + 1.334534 \times 10^{-2} T + 11.71189) \frac{1-p}{1+2.5p}, \quad (9)$$

where T is temperature in K, and p is fuel porosity. Fuel porosity is calculated using fission gas induced swelling:

$$p = \frac{\left(\frac{\Delta V}{V_0} \right)_g}{\left(\frac{\Delta V}{V_0} \right)_g + 1}, \quad (10)$$

4.3 Fuel Creep

Fuel creep rate is temperature, stress, porosity, and fission rate dependent and is calculated using published methodology.¹³

$$\begin{aligned} \epsilon' = & 5000 \times (1 + 7.9p + 470p^2) \sigma \exp\left(-\frac{52000}{RT}\right) + \\ & + 6(1 - p^{0.67})^{-0.8} \sigma^{4.5} \exp\left(-\frac{52000}{RT}\right) + 7.7 \times 10^{-23} \sigma F', \end{aligned} \quad (11)$$

where p , σ , R , T , F' are porosity, stress, gas constant, temperature, and fission rate respectively.

4.4 Cladding Creep

Cladding creep rate is temperature and stress dependent and is calculated using published methodology.¹⁴

$$\epsilon' = 1.17 \times 10^9 \sigma^2 \exp\left(-\frac{83142}{1.987T}\right) + 8.33 \times 10^9 \sigma^5 \exp\left(-\frac{108276}{1.987T}\right) \quad (12)$$

where σ , and T , are stress and temperature respectively.

4.5 Coupling Between the Models to Capture the Multiphysics Phenomena

Examination of equations presented above reveals complex interdependence of fuel performance parameters and behavior models. To capture this interdependence, the equations were coupled in a manner depicted in Figure 3, utilizing BISON's advanced object oriented architecture, and producing a truly multiphysical model of the metallic fuel swelling and deformation. The implementation of the model was carried out by the present study specifically to address FCRD metallic fuel development challenges. By accounting for the effects of FCMI and temperature on swelling, and by using extensive coupling, the present model constitutes a significant advancement of the generic version of the BISON code distributed to users.

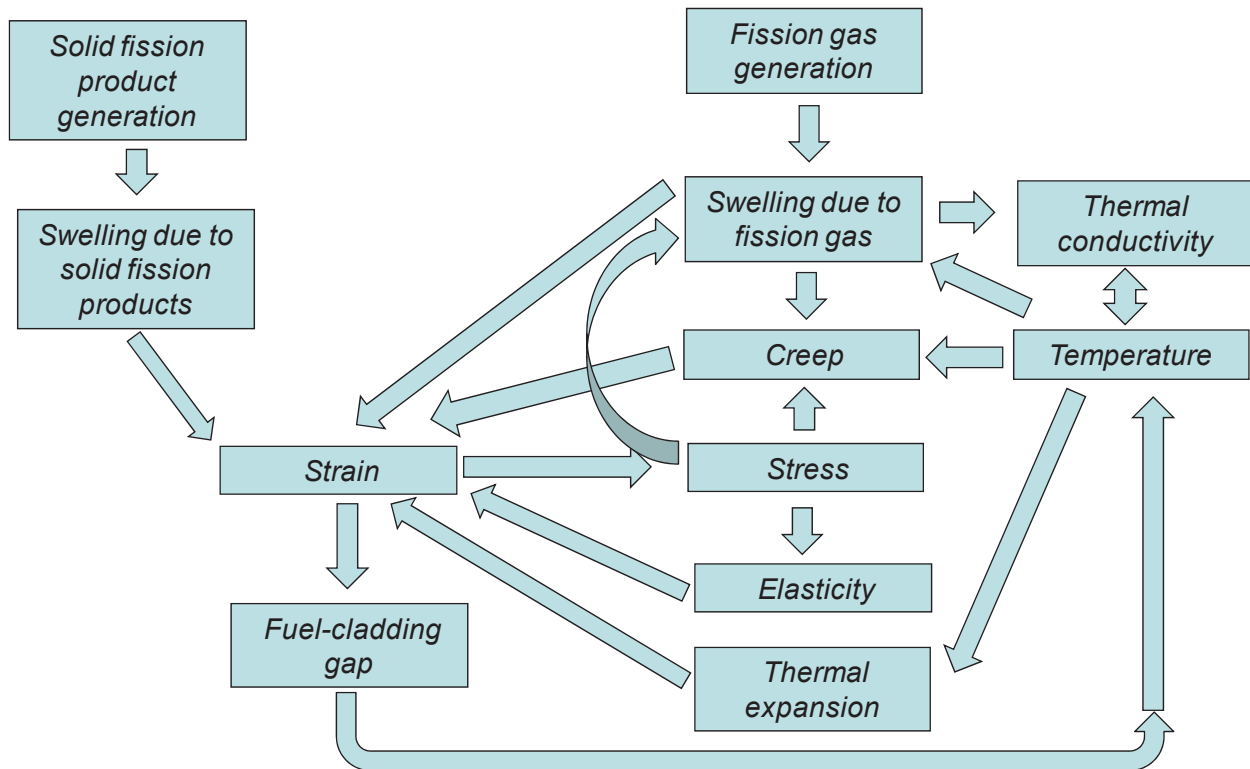


Figure 3. Coupling between the models to capture the multiphysics phenomena

5. CALCULATION PROCEDURE

Execution of the fuel performance calculation using BISON requires two problem-specific files: (1) a mesh file that contains two-dimensional description of the problem geometry, and (2) an input file that includes information on material properties, power history, boundary conditions and parameters that control numerical algorithms in BISON.

5.1 Mesh Files

Mesh files were created using CUBIT Version 12.1 geometry and mesh generation toolkit.¹⁵ The mesh consisted of two blocks: the fuel slug and the cladding. Establishing two blocks in the mesh allows assigning specific material properties to each block. Heat generation rate is assigned to the fuel block. The key parameters of the mesh are given in Table 2.

Table 2. Key parameters of the mesh used for the rodlet assembly model.

Block	Component	Number of elements	Element type
1	Cladding	2390	QUAD8
2	Fuel slug	2000	QUAD8

An image of the QUAD8 used in the model element is shown in Figure 4. This is a quadratic order element featuring eight nodes located in the corners and on the edges.

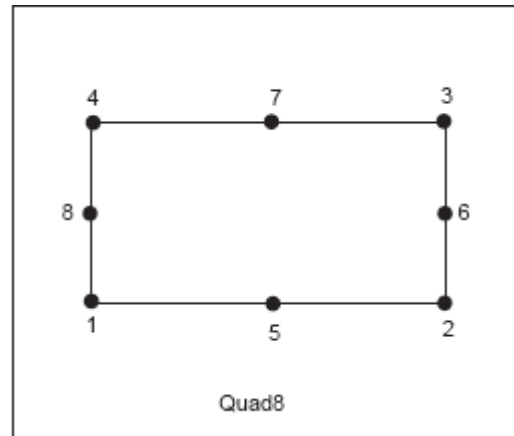


Figure 4. A diagram of the QUAD8 element used in the rodlet assembly mesh.

Rodlet assembly dimensions used to generate metal rodlet mesh files are listed in Table 3.

Table 3. Rodlet assembly dimensions used to generate metal rodlet mesh files.

Configuration	Annular	Solid	Annular	Solid
SD, %	55	55	75	75
Fuel slug outer diameter, mm	4.86	3.66	4.86	4.26
Fuel slug inner diameter, mm	3.25	0	2.47	0
Fuel slug length, mm	38.05			
Cladding outer diameter, mm	5.84			
Cladding inner diameter, mm	4.93			
Plenum to fuel ratio	2.34			

The fuel/cladding gap was not meshed. Instead, temperature drops across these gaps were calculated from the thermal conductivity of the gap material and the heat flux.

5.2 Input Files

Four input files were developed by the present study to include the base design featuring annular fuel slug with 55% SD, solid fuel slug with 55% SD, annular fuel slug with 75% SD, and solid fuel slug with 75% SD. Because the geometrical differences between the analyzed cases are reflected in the mesh files, the input files for the four cases are identical with the exception of the volumetric fission rate. The volumetric fission rate of 10.38×10^{19} fissions/m³-s and 7.64×10^{19} fissions/m³-s were used for the 55% and 75% SD cases respectively. This corresponds to the linear heat generation rate of 350 W/cm, which is typical for the AFC-3A irradiation experiment.⁵

The list of material properties used in this study is given in Table 4.

Table 4. Material properties used in the present study.

	Thermal Conductivity (W/m-K)	Specific Heat (J/kg-K)	Density, (kg/m ³)	Young's modulus (Pa)	Thermal Expansion, (1/K)	Poisson Ratio
Fuel	Temperature and porosity dependent	330	15730	7.5e10	1.8e-5	0.3
Cladding	22	330	6551	1.88e11	1.2e-5	0.236
Helium	0.3	Not used				
Sodium	61					

A convective heat flux boundary condition was applied to the surface of the cladding. The coolant temperature of 325 K and the film coefficient of 4000 W/m²-K were used.

5.3 Assumptions and Limitations

Assumptions were required to accomplish the demonstration objective with the effort and time allotted for this work. The major assumption and limitations are as follows:

- “Glued” contact between the fuel and the cladding, i.e., axial movement of the fuel relative to the cladding is not allowed after fuel and cladding come in contact
- Fuel cladding chemical interaction is not considered
- Increase of fuel thermal conductivity due to sodium infiltration is not considered
- Power generation in the fuel is uniform
- The experiment basket and capsule are not included in the model.

5.4 Computer Platforms and Software Version

BISON is designed to run on a variety of UNIX and Mac-based computer platforms. All the simulations described in this study were run on a MacPro workstation (model name: Mac Pro; model identifier: MacPro 5.1; operating system: Mac OS X 10.6.7; processor name: 6-Core Intel Xeon; processor speed: 2.93 GHz; number of processors: 2; total number of cores: 12), typically using all twelve cores. In all cases, the parallel nature of the calculation is handled completely by the software, with the user simply specifying the number of processors at execution time.

All simulations described in this report were run using BISON at revision number 11212. BISON version control is performed by the Fuel Modeling and Simulation Department of the INL.

5.5 Code Verification

Verification tests for the kernels/operators used in this work were successfully executed after the code was compiled. This implies that the agreement was confirmed between the numerical solution produced by the BISON and an analytical solution for each verification test. BISON verification tests are developed, maintained, and archived by the Fuel Modeling and Simulation Department of the INL.¹⁶ Full verification and validation of BISON has not occurred because the code is in a development stage.

6. RESULTS

6.1 Fuel Swelling and Fission Gas Release

The key question to be answered by the irradiation testing of the annular U-10Zr fuel in the AFC-3A test is whether the fuel will swell inward and fill the annulus, or the fuel will swell outward and cause undesirable cladding stress and deformation. Given the behavior models and material properties described above, the fuel performance analysis, executed using BISON code, revealed that the fuel will swell inward, and partially fill the annulus during 201 days of irradiation at the linear power of 350 W/cm. Figure 5 shows the axial cross-section of the fuel and the cladding before and after irradiation. Fuel swelling is evident in Figure 5, as manifested by the reduction of the fuel annulus and the fuel elongation.

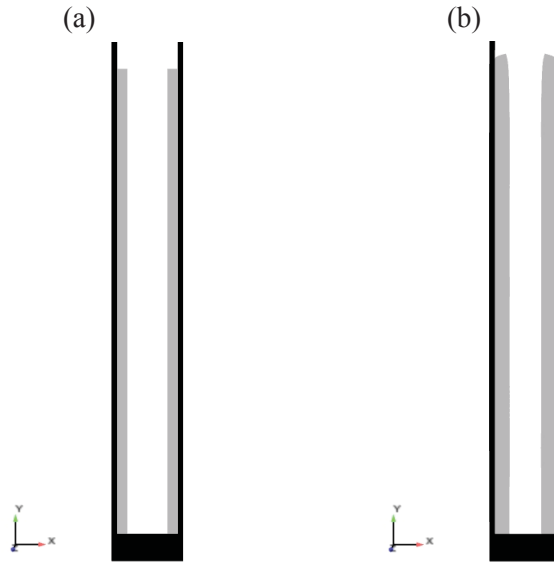


Figure 5. Results for the simulation of the AFC-3A annular U-10Zr fuel irradiation where (a) shows fuel and cladding geometry before the irradiation, (b) shows fuel and cladding geometry after irradiation.

Recognizing that fuel annulus diameter, fuel outer diameter (OD), and cladding OD will be measured during post irradiation examination, the predicted values for these parameters are shown in Figure 6. Evidently, essentially no increase of the fuel and cladding OD is predicted. The fuel annulus diameter shows a reduction from 3.25 mm to 2.56 mm. Axial elongation of the fuel is another parameter that will be measured during post irradiation examination. Predicted axial elongation of the fuel is shown, as a function of burnup, in Figure 7.

Examination of the Figure 7 reveals three distinct swelling regimes experienced by the annular fuel in the AFC-3A experiment. The first regime occurs before the fuel-cladding gap closure, when the fuel is unconstrained and exhibits the highest swelling rate. The second regime begins after the gap closure, and continues until the gas induced swelling of the fuel reaches the threshold of 33% when the closed porosity interconnects and the fission gas is released. The swelling rate is lower during the second regime due to increase of the compressive hydrostatic stress in the fuel, caused by pellet cladding mechanical interaction (PCMI). The increase of the compressive hydrostatic stress in the fuel is illustrated in Figure 8. In Figure 8, the “+” sign of the stress value indicates tension, and the “-” sign indicates compression. Therefore, the PCMI occurring after the gap closure at about 0.25% burnup, causes hydrostatic stress to change from -0.14 MPa to -3.5 MPa, which implies an increase of the compression. Finally, the third regime begins after the fission gas is released, and is characterized by the lowest swelling rate due solid fission products only. This regime is unaffected by the hydrostatic stress in the fuel, as the solid fission products are incompressible.

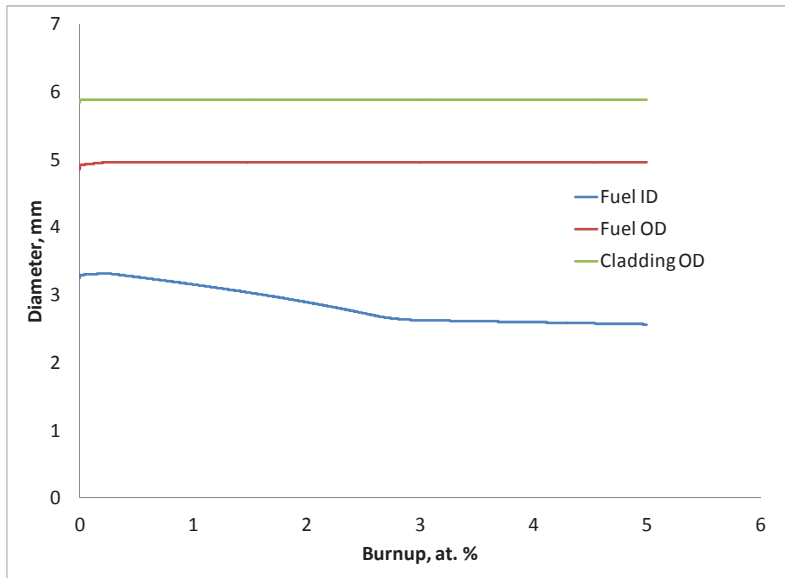


Figure 6. Evolution of the fuel annulus, fuel outer diameter, and cladding outer diameter at the fuel mid-plane as a function of burnup.

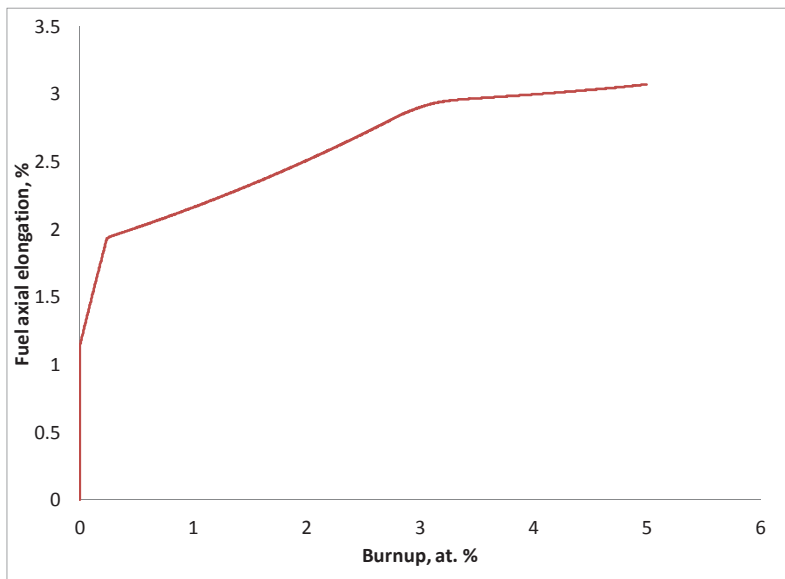


Figure 7. Fuel axial elongation as a function of burnup.

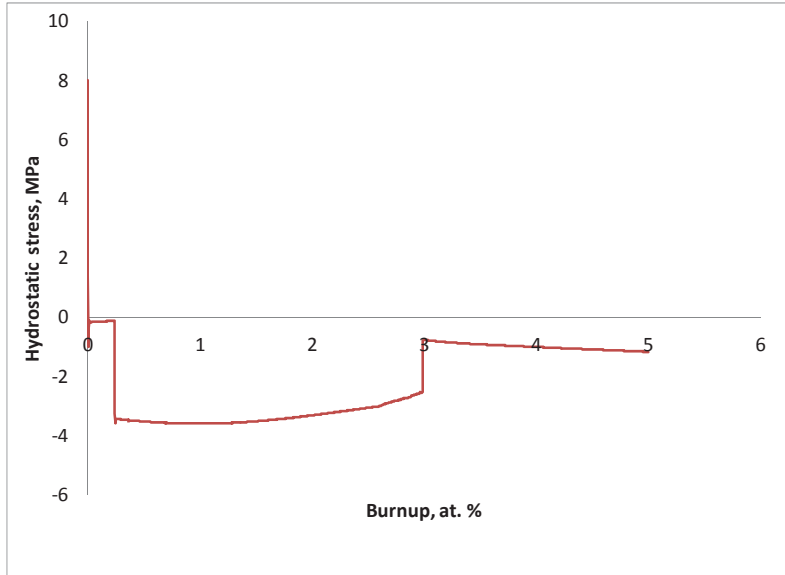


Figure 8. Evolution of the hydrostatic stress with the fuel with burnup. The data is for an element located at the midplane on the exterior surface of the fuel slug.

A spike in hydrostatic stress at the time of the reactor startup can be noticed in Figure 8. This spike is explained by the thermal expansion stresses in the fuel that occur due to temperature difference between the hotter inner regions at the fuel, and colder regions on the fuel exterior. The thermal expansion stress is quickly relaxed by the irradiation induced creep of the fuel.

The integral fuel swelling ($\Delta V/V_0$) as a function of burnup is shown Figure 9. The plot shows that the fuel exhibits higher swelling rate until it reaches approximately 2.6% burnup. After that, the swelling rate is reduced significantly. It was predicted, that interconnection of the fission gas porosity occurs at approximately 2.6% burnup, resulting in the fission gas release. Fission gas release as a function of burnup is shown in Figure 10.

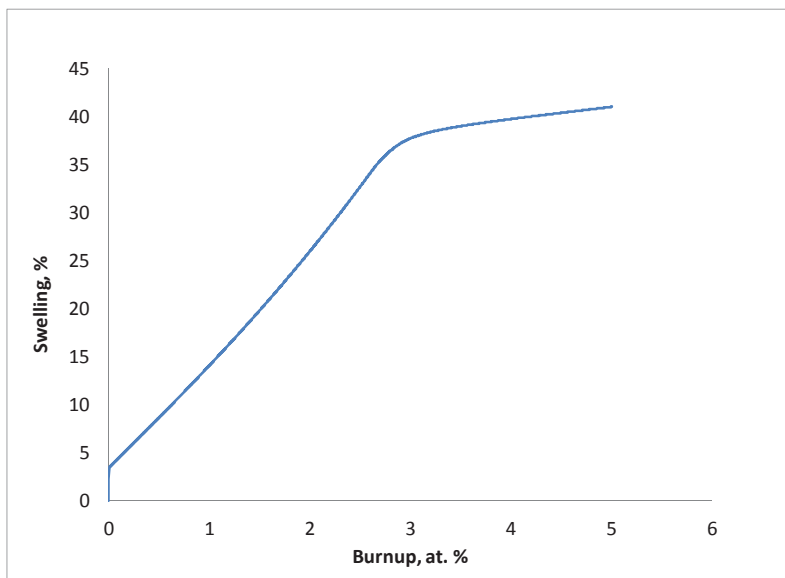


Figure 9. Fuel swelling as a function of burnup.

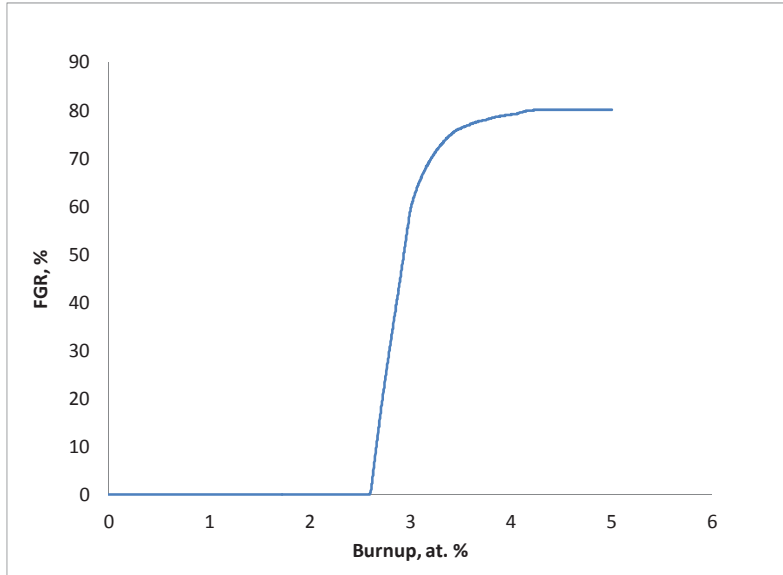


Figure 10. Fission gas release as a function of burnup.

6.2 Fuel and Cladding Temperature

The history of the peak fuel and cladding temperatures is shown in Figure 11. The maximum fuel temperature is experienced in the beginning of irradiation, prior to closure of the fuel-cladding gap. Gap closure results in the fuel temperature drop. As the thermal conductivity of the fuel degrades with irradiation, the fuel temperature shows a moderate increase until porosity interconnection occurs. Once the porosity interconnects, the temperature remains nearly constant, since no additional porosity is generated when the newly generated fission gas is instantly released through the interconnected porosity.

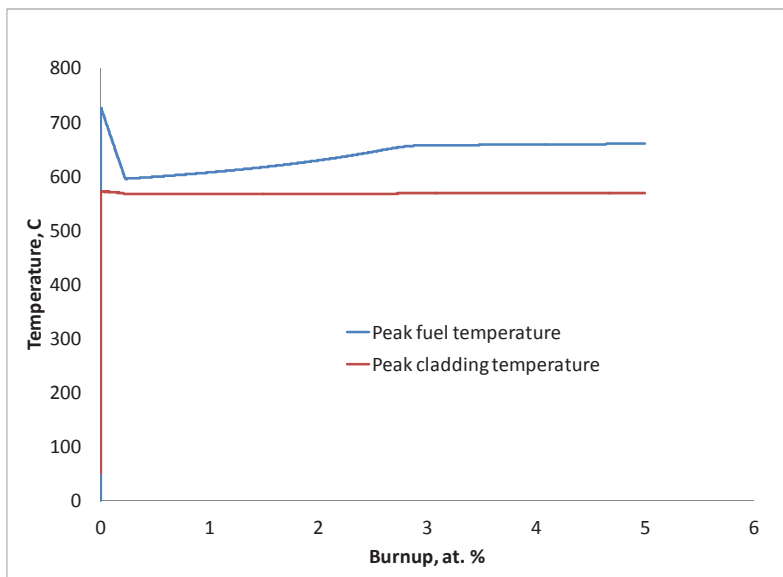


Figure 11. History of the peak fuel and peak cladding temperatures.

6.3 Cladding Stress

Evolution of the cladding mid-wall hoop stress at the fuel mid-plane is shown in Figure 12. Results show that the mid-wall cladding hoop stress insignificant compared to the HT-9 yield stress of 620-633 MPa.¹⁷ The plot indicates that the cladding hoop stress increases after fuel-cladding contact. The increase is followed by a notable stress relaxation that is owed to the high creep rate of the fuel, and availability of the free volume of the fuel annulus. After the fission gas is released, the cladding hoop stress begins to increase due to increasing plenum pressure, and PCMI caused by the buildup of the solid fission products.

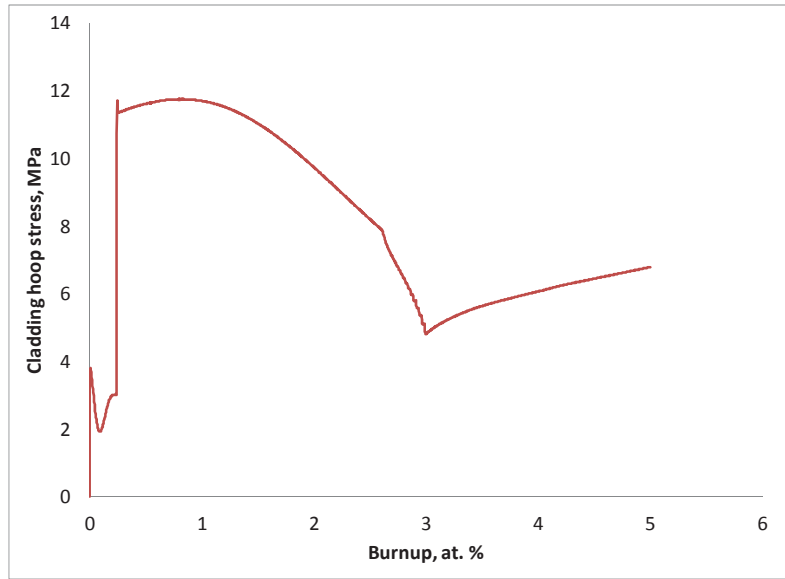


Figure 12. Evolution of the cladding mid-wall hoop stress at the fuel mid-plane.

6.4 Plenum Pressure

Owing to a very large plenum of the AFC-3A rodlets, the plenum pressure remains very low during the experiment. As shown in Figure 13, plenum pressure does not exceed 1 MPa at the end of irradiation. This is well below the rodlet programmatic confidence pressure limit of 4170 psi (28.75 MPa).¹⁸ The increase in plenum pressure evident in Figure 13 is due to the fission gas release predicted at 2.6% burnup.

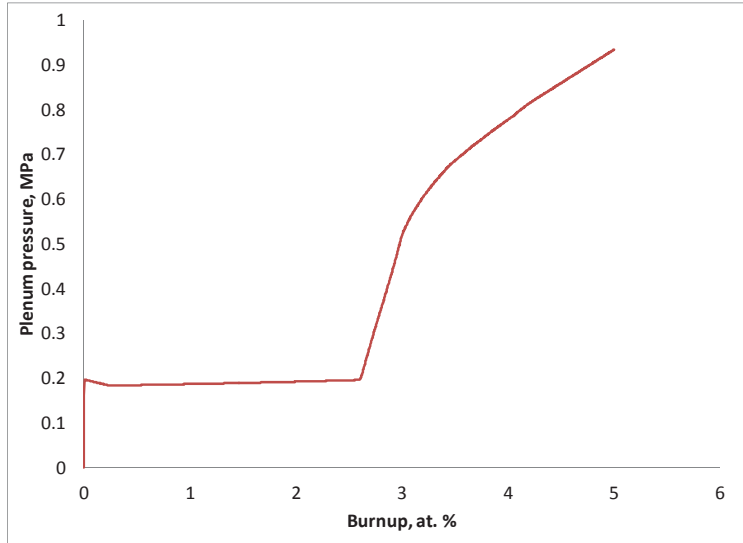


Figure 13. Plenum pressure history.

6.5 Dominant Fuel Creep Mechanism

6.5.1 Beginning of Life, Non-porous Fuel

As evident from Equation (11), the fuel creep is calculated as a sum of the thermal and irradiation induced creep terms. The thermal creep rate depends on stress, temperature, and porosity of the fuel, and the irradiation induced creep depends on stress, temperature, and fission rate. Behavior of the Equation (11), including thermal and irradiation creep terms, at the fuel temperature of 600C and 726C, fission rate of 10.381×10^{19} fissions/m³-s, and stress ranging from 0.1 to 10 MPa is illustrated in Figure 14 and Figure 15. This result is for the non-porous fuel representative of the fuel at the beginning of life. Comparison of Figure 14 and Figure 15 shows that at the temperature of 600C the irradiation induced creep dominates the creep behavior, while at 726C the thermal creep is dominating. This result suggests that both thermal and irradiation creep measurements are needed to accurately describe fuel deformation and neither of the creep modes can be neglected.

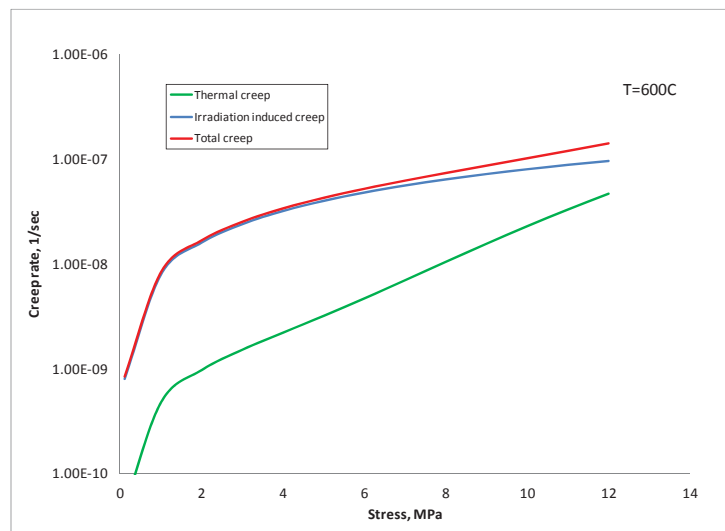


Figure 14. Contributions from thermal and irradiation induced creep to the total creep rate of the fuel at 600C, non-porous fuel.

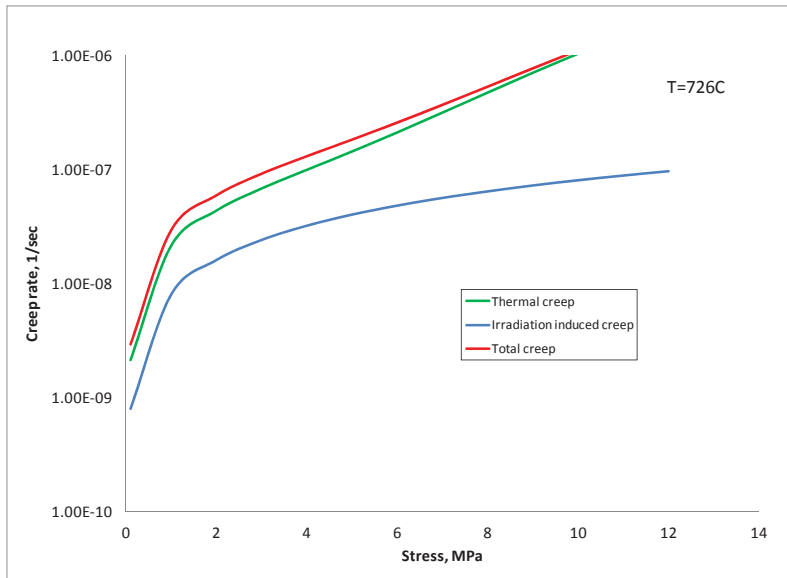


Figure 15. Contributions from thermal and irradiation induced creep to the total creep rate of the fuel at 726C, non-porous fuel.

6.5.2 Effect of Fuel Porosity

Plots similar to Figure 14 and Figure 15 were obtained for the fuel having 24% porosity representing the maximum porosity fuel can attain before the fission gas bubbles begin to interconnect. The plots accounting for the effect of porosity on the creep rate are shown in Figure 16 and Figure 17. The fission gas porosity accelerated the thermal creep of the fuel to the extent that the irradiation induced creep becomes insignificant and can be neglected.

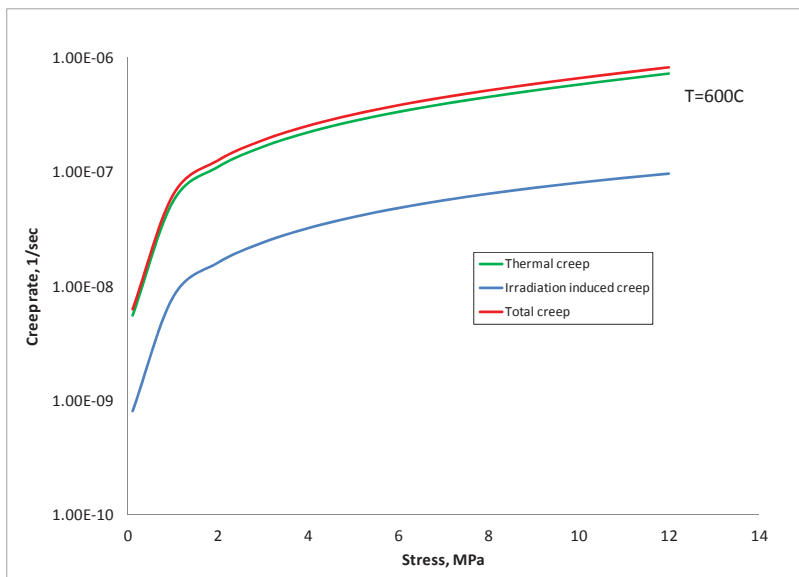


Figure 16. Contributions from thermal and irradiation induced creep to the total creep rate of the fuel at 600C, fuel porosity 26%.

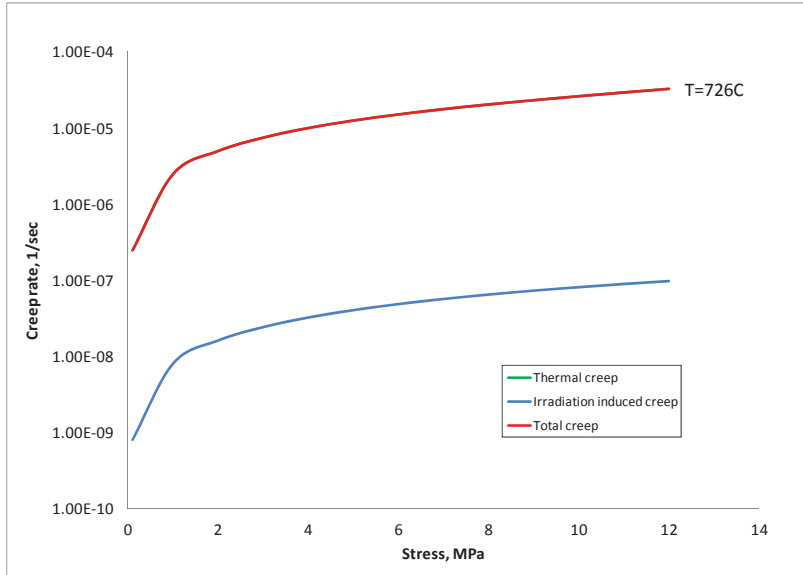


Figure 17. Contributions from thermal and irradiation induced creep to the total creep rate of the fuel at 726C, fuel porosity 26%.

6.6 Fuel Creep Strain

Fuel creep strain at the end of irradiation is shown in Figure 18. Evidently, the creep strain reaches values up to 0.52 (52%) as a result of high creep rate prescribed by the Equation (10). Noting that fuel swelling is isotropic, it appears that it is the fuel creep phenomenon that is responsible for relocation of the fuel into the annulus. This is substantiated by the observation of the maximum creep strain on the inner surface of the fuel, manifested by the red color in Figure 18.

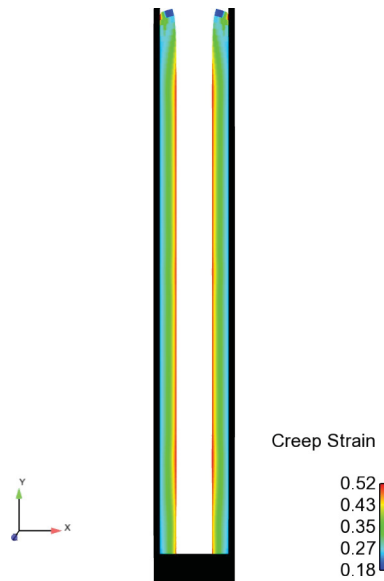


Figure 18. Fuel creep strain at the end of irradiation.

6.7 Comparison with the Annular 75% SD U-10Zr Fuel

Irradiation of the annular 75% SD U-10Zr fuel is among AFC-3 experiments proposed for insertion in FY-2013.¹⁹ Irradiation performance of this experiment was modeled using the same methodology. It was assumed that the 75% SD fuel would operate at the same linear power of 350 W/cm and the experiment duration would be 201 days. Because the volume of the fuel is higher in the case of the 75% SD fuel, it would reach lower burnup if irradiated at the same power and for the same irradiation time as the 55% SD fuel. It was found, that, despite the increase in the SD, the fuel is expected to swell inward and partially fill the annulus, as in the case of the annular 55% SD fuel. Fuel and cladding geometry before and after irradiation is shown in Figure 19.

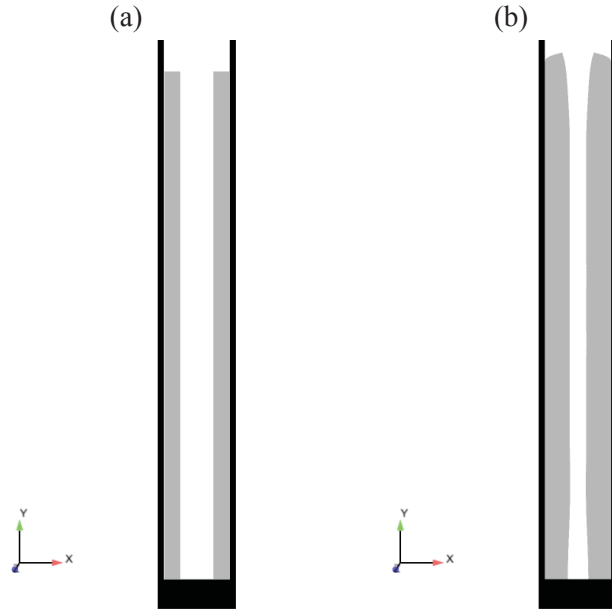


Figure 19. Results for the simulation of the annular 75% U-10Zr fuel irradiation where (a) shows fuel and cladding geometry before the irradiation, (b) shows fuel and cladding geometry after irradiation.

Comparison of the swelling of the annular 55% and 75% SD fuel is shown in Figure 20. As illustrated in Figure 20, the fuel with higher SD exhibits lower swelling rate. This is explained by the higher compressive hydrostatic stress that was predicted in the annular 75% SD fuel, as shown in Figure 21. Due to the lower swelling rate, the annular 75% SD fuel exhibits slightly lower fission gas release as depicted in Figure 22. The peak fuel temperature is slightly higher in the annular 75% SD fuel case, as evidenced in Figure 23. Higher fuel temperature is due to the effect of the geometric considerations on the heat conduction within the annular fuel, specifically, the decrease of the fuel inner diameter while keeping the fuel outer diameter and linear heat generation rate constant. Overall, the simulation suggests a very similar behavior of the annular fuels with 75% and 55% SD when both are irradiated at 350 W/cm for 201 days.

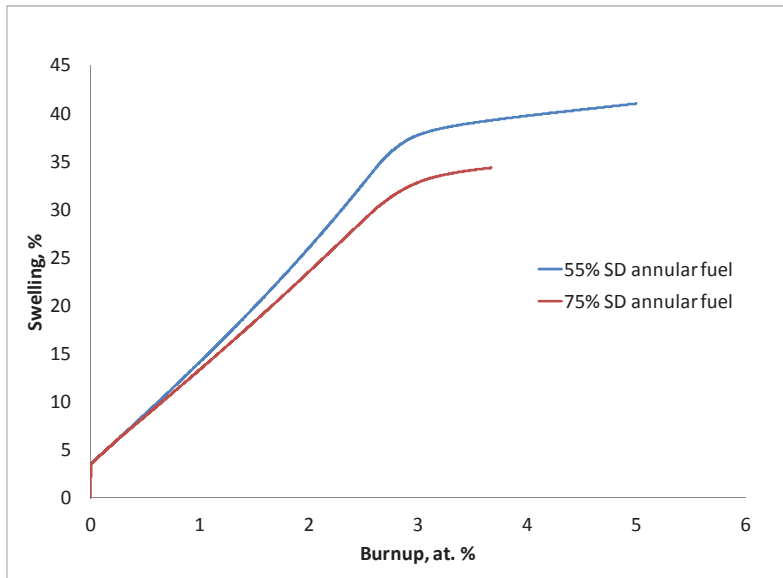


Figure 20. Comparison of the swelling of the annular 55% and 75% SD fuel.

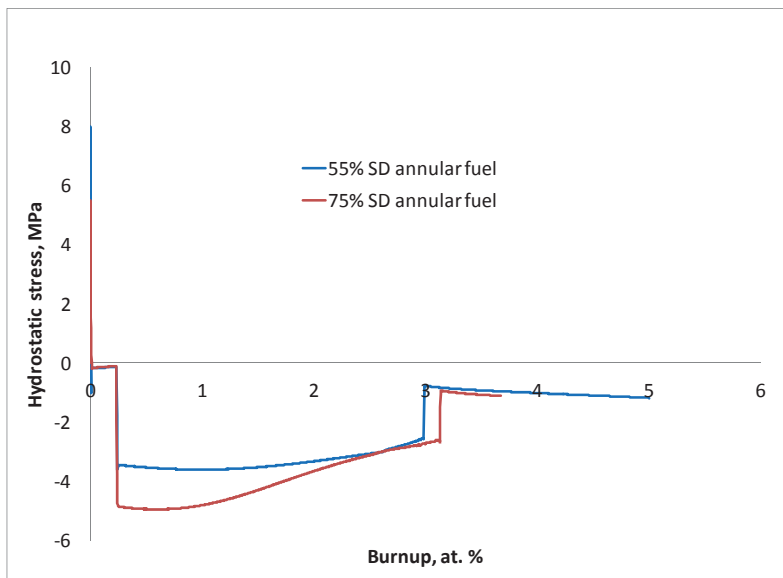


Figure 21. Comparison of the hydrostatic stress in the annular 55% and 75% SD fuel.

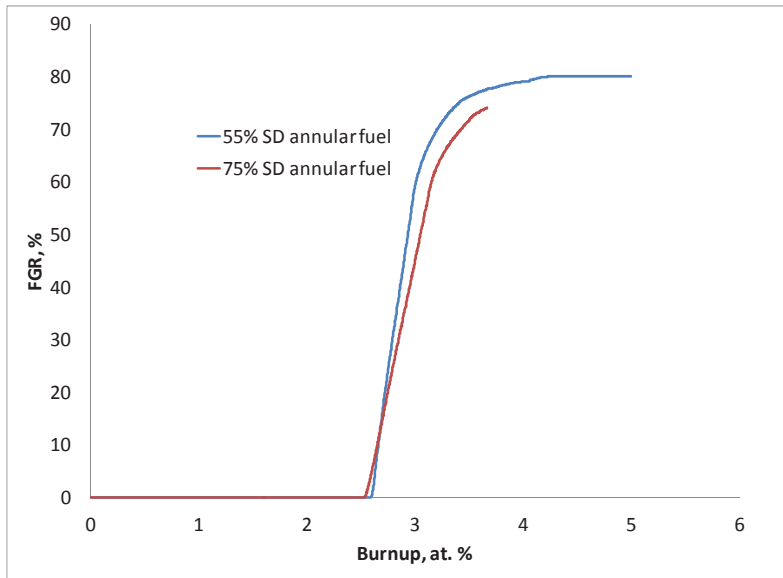


Figure 22. Comparison of the fission gas release in the annular 55% and 75% SD fuel.

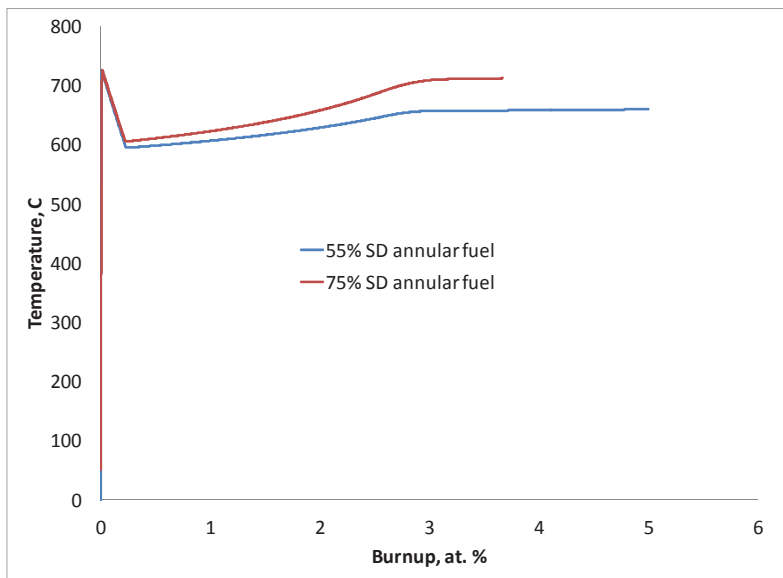


Figure 23. Comparison of the peak fuel temperature in the annular 55% and 75% SD fuel.

6.8 Comparison with the Solid 55% SD U-10Zr Fuel

To understand the benefits of using annular fuel and to isolate phenomena responsible for the differences in behavior, a simulation of the irradiation of the solid 55% SD U-10Zr fuel was performed, and results were compared with the annular 55% SD U-10Zr fuel. As in the other cases, it was assumed that the fuel would operate at the linear heat generation rate of 350 W/cm for 201 days. Fuel and cladding geometry before and after irradiation for the solid 55% U-10Zr fuel is shown in Figure 24. Figure 24 reveals the extent of the fuel swelling and shows that the fuel-cladding gap will not close during the irradiation.

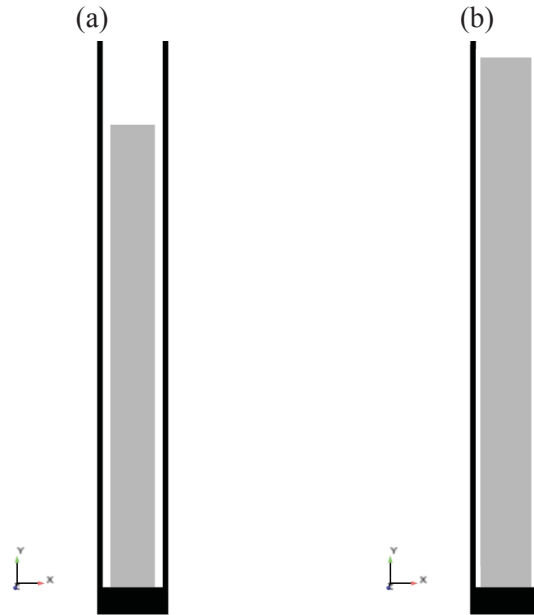


Figure 24. Fuel and cladding geometry before and after irradiation for the solid 55% U-10Zr fuel.

Comparison of the swelling of the solid and annular fuel as a function of burnup is shown Figure 25. It is apparent, that during the period from the start up to the porosity interconnection event, the swelling rate of the solid fuel is greater than that of the annular fuel.

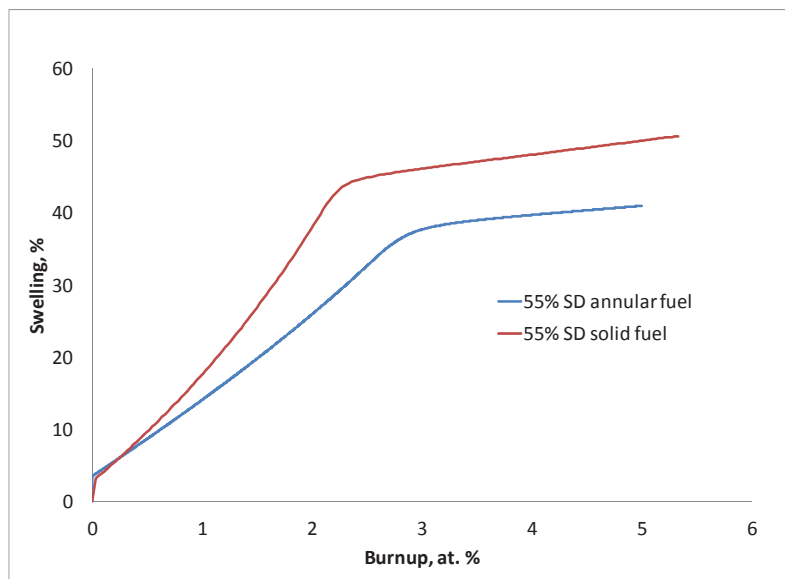


Figure 25. Swelling comparison of the solid and annular fuels, both fuels 55 %SD.

The difference in the swelling rate is because compared to the annular fuel; the solid fuel operates at a greater temperature, shown in Figure 26, and a lower compressive hydrostatic stress, shown in Figure 27. The operating temperature of the solid fuel is higher due to geometric considerations, and the compressive hydrostatic stress is lower due to the lack of the fuel cladding mechanical interaction (FCMI) during the irradiation period under consideration. A marked difference is observed between the axial elongations of the annular and solid fuels. Predictions show axial elongation of the solid fuel reaching 14.5% at the end of irradiation, in contrast with only 3.1% axial elongation of the annular fuel as shown in Figure 28. The

difference is due to the axial constraint that is provided by the FCMI that is expected to begin early in life of the annular fuel and continue throughout the irradiation. It should be noted that the FCMI model assumes “glued” contact between the fuel and the cladding, once the fuel swells and the gap is closed. Post irradiation examination results would be very useful to assess the validity of this assumption. Specifically, an underprediction of the fuel axial growth would point to the fact that some slippage of the fuel relative to the cladding occurs after the onset of the FCMI.

In the solid fuel, the higher swelling rate results in an earlier onset of the fission gas release as shown in Figure 29. The fission gas release onset is predicted at the 2.04% burnup, in contrast with the 2.6% burnup in the annular fuel.

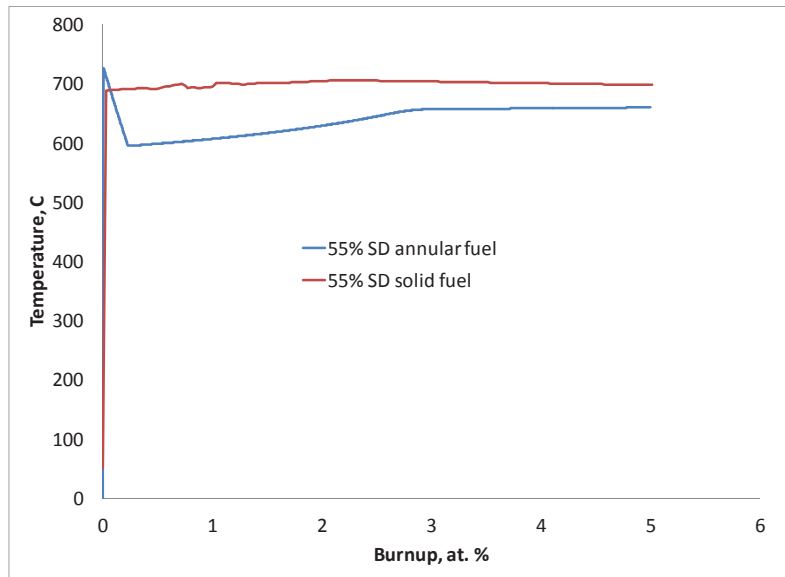


Figure 26. Peak fuel temperature comparison of the solid and annular fuels, both fuels 55% SD.

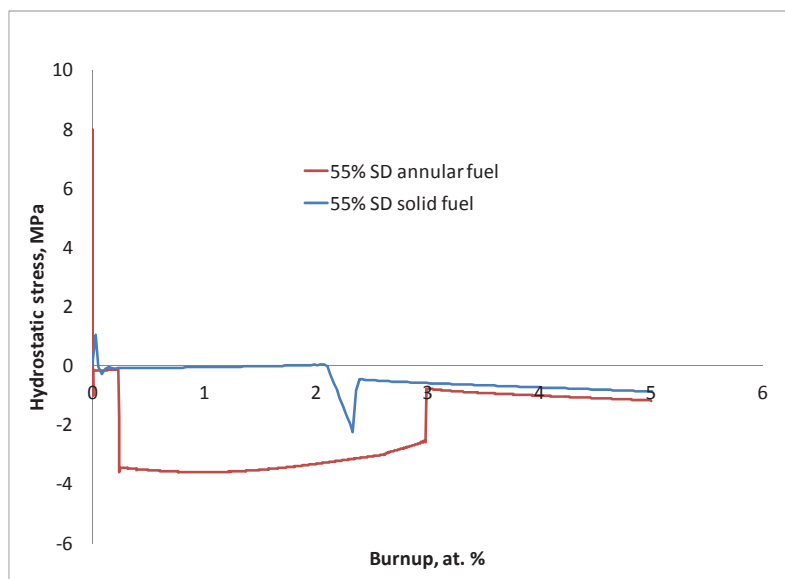


Figure 27. Hydrostatic stress comparison in the solid and annular fuels, both fuels 55% SD.

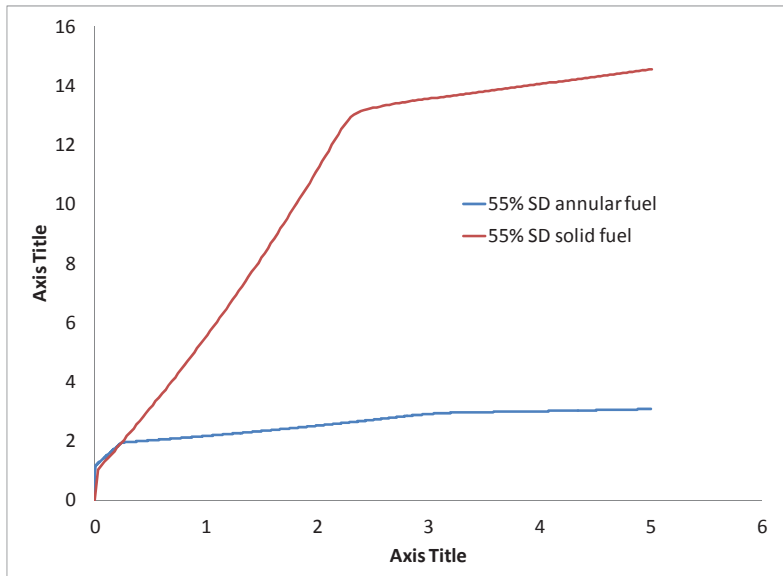


Figure 28. Comparison of the axial fuel elongation of the solid and annular fuels, both fuels 55 %SD.

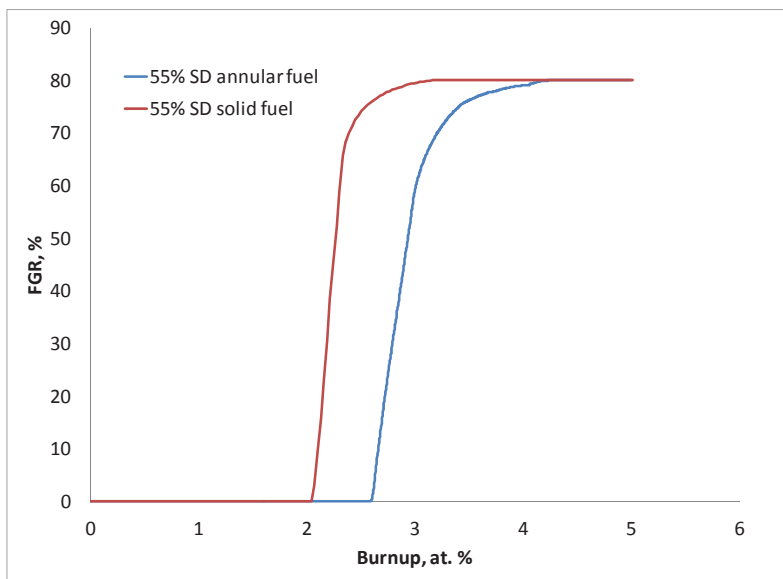


Figure 29. Fission gas release comparison in the solid and annular fuels, both fuels 55% SD.

Fuel performance comparison of the 55% SD annular and solid fuels operating at the same power levels, points to the reduced fission gas induced swelling rate, and reduced axial elongation as obvious advantages of the annular fuel design. The advantage of the reduced axial elongation may be particularly attractive, as the axial fuel elongation is responsible for the negative reactivity feedback during reactor operation. Furthermore, an uncertainty associated with the high fuel axial elongation complicates the reactor core design, particularly for the high burnup applications. As mentioned above, the reduced swelling rate is owed to the mechanical constraint of the fuel by the cladding that begins shortly after the startup and continues throughout the irradiation. Early fuel-cladding contact in the annular fuel case is expected to yield an earlier onset of the fuel cladding chemical interaction (FCCI), a negative phenomenon. FCCI modeling is beyond the scope of the present study, partly because the duration of the irradiation test is fairly short for the development of significant FCCI.

7. CONCLUSIONS

The objective of the present study was to predict the outcome of the AFC-3A annular U-10Zr fuel irradiation experiment. Specifically, the study attempted to predict whether the annular fuel will swell inward and fill the annulus, or swell outward resulting in an undesirable cladding deformation.

It was predicted that both 55% and 75% annular fuels operating at 350 W/cm for 201 days will swell inward and partially fill the annulus which signifies a positive outcome of the experiment. The driving mechanism for such behavior is the fuel creep under the compressive stress exerted on the fuel by the cladding as a result of the fuel cladding mechanical interaction.

Comparison with the solid fuel revealed that the annular fuel is expected to swell less early in life due to the mechanical constraint provided by the cladding. Furthermore, mechanical constraint is expected to yield a marked reduction of the axial elongation of the annular fuel as compared to the solid fuel. The prediction is based on the assumption that the annular fuel is not capable of moving axially relative to the cladding after the two come in contact. Post irradiation examination results would be very useful to assess the validity of this assumption. Specifically, the underprediction of the axial fuel growth would point to the fact that some slippage of the fuel relative to the cladding occurs after the onset of the FCMI.

As the fuel creep plays the major role in the deformation of the annular fuel, the contributions from the thermal and irradiation induced creep to the total creep rate of fuel were examined to provide guidance for possible creep testing experiments of the fuel (separate effect tests). It was found that the irradiation induced creep dominates deformation of the fresh fuel at low temperatures. At high temperatures, and in the case of porous fuel, the thermal creep of the fuel becomes dominant and irradiation induced creep can be neglected. Fission gas induced porosity seems to accelerate fuel creep drastically. Recognizing the sensitivity of the fuel creep to the porosity, additional studies exploring this phenomenon and verifying published equations either experimentally or through computation may benefit the understanding of the annular fuel behavior.

8. REFERENCES

1. Williamson, R. L. et al., "Multidimensional multiphysics simulation of nuclear fuel behavior", *Journal of Nuclear Materials*, 423 (2012) 149-163.
2. Gaston, D., "MOOSE: A parallel computational framework for coupled systems of nonlinear equations," *Nuclear Engineering and Design* 239 (2009) 1768–1778.
3. Wright A. E. et al., Development of Advanced Ultra-High Burnup SFR Metallic Fuel Concept - Project Overview, *Transactions of the American Nuclear Society*, Vol. 106, Chicago, Illinois, June 24–28, 2012.
4. Jones, W.F, AFC-3 Rodlet Thermal Evaluation, Engineering Calculation and analysis report ECAR-1493, Idaho National Laboratory, 2011.
5. Glass C.R, Chang G. R., ATR Cycle 151A As-Run and 151B Projected Physics Evaluations for the AFC-3A and -3B Experiments in the A-10 and A-11 Positions, Engineering Calculation and analysis report ECAR-1816, National Laboratory, 2012.
6. AFC-3 Annular Fuel Rodlet Assembly, Idaho National Laboratory Engineering Drawing 603235, 2011.
7. AFC-3 Annular Fuel Details, Idaho National Laboratory Engineering Drawing 603233, 2011.
8. Barnes R. S., A Theory of Swelling and Gas Release for Reactor Materials, *Journal of Nuclear Materials*, 11 (1964) 135-148.
9. Karahan A., Modeling of Thermo-Mechanical and Irradiation Behavior of Metallic and Oxide Fuels for Sodium Fast Reactors, Thesis, Massachusetts Institute of Technology 2009.
10. Churchman A. T. et al., Effects of Heat and Pressure on the Swelling of Irradiated Uranium, *Nuclear Energy*, 7 (1958) 88-96.
11. T. Ogata et al., Development and Validation of ALFUS: An irradiation Behavior Analysis Code for Metallic Fast Reactor Fuels, " *Nuclear Technology* 128 (1999) 113-123.
12. Billone M. C. et al., Status of the Fuel Element Modeling Codes for Metallic Fuels, *Proc. Int. Conf. Reliable Fuels for Liquid Metal Reactors*, American Nuclear Society Tucson, Arizona (1986).
13. Kutty T. R. G. et al., Creep behaviour of δ -phase of U–Zr system by impression creep technique, *Journal of Nuclear Materials* 408 (2011) 90–95.
14. Crawford et al., AFCI Fuel Irradiation Test Plan, Test Specimens AFC-1Æ and AFC-1F, INEEL/EXT-03-01362, 2003.
15. <http://cubit.sandia.gov>
16. Idaho National Laboratory internal link <https://hpcsc/data/trac/FPCP/browser>.
17. Hosemann P., An exploratory study to determine applicability of nano-hardness and micro-compression measurements for yield stress estimation, *Journal of Nuclear Materials* 375 (2008) 135-143.
18. Chichester, H., AFC-3A and 3B Pressure Estimates, Engineering Calculation and analysis report ECAR-1666, National Laboratory, 2011.
19. Barrett K., Project Execution plan for the Fuel Cycle Research and Development AFC-3 Irradiation Experiments in the ATR, PLN-3608, Idaho National Laboratory, 2012.